Carbon-Coated Porous Aluminum Oxides Used as Spacer Overlayers to Reduce Secondary Electron Emission for Field Emission Display Applications

2013 Jpn. J. Appl. Phys. 52 075801

(http://iopscience.iop.org/1347-4065/52/7R/075801)

Japanese Journal of Applied Physics **52** (2013) 075801 **REGULAR PAPER**
http://dx.doi.org/**10.7567/JJAP.52.075801**

Carbon-Coated Porous Aluminum Oxides Used as Spacer Overlayers to Reduce Secondary Electron Emission for Field Emission Display Applications

Tung-Yuan Yu[1], Fu-Ming Pan[1]*, Cheng-Li Chen[1], Te-Ming Chen[2], Tsung-Han Chen[2], Chih-Che Kuo[2], and Ting-Li Lin[2]

[1]*Department of Materials Science and Engineering, National Chiao-Tung University, Hsinchu, Taiwan 30010, R.O.C.*
[2]*AU Optronics Corporation, Hsinchu Science Park, Hsinchu, Taiwan 30078, R.O.C.*
E-mail: fmpan@faculty.nctu.edu.tw

Received March 5, 2013; revised April 16, 2013; accepted May 12, 2013; published online June 19, 2013

Porous surface structures can mitigate the charging effect of vacuum spacers of field-emission flat panel display due to the abundance of secondary electrons (SEs) emitted from the spacers during field emission display (FED) operation. In this study, we fabricated porous anodic aluminum oxide (AAO) overlayers on glass substrates to examine the effect of carbon deposition on the reduction of SE emissions. This paper reports that uniform AAO overlayers can be simultaneously prepared on both sides of a glass plate $2 \times 10\,cm^2$ in size. The SE emission of the AAO overlayer was examined by using an Auger electron microscope. When a small amount of carbon is evaporation-deposited on the as-prepared AAO overlayer, the SE emission efficiency is significantly decreased and the reduction in the SE emission is ascribed to the low SE yield of the carbon deposit and the suppression of SE escape from the narrowed pore channels. However, a heavy deposition of carbon results in a smaller surface roughness of the AAO overlayer, thereby increasing SE emission. The carbon-coated AAO overlayer demonstrates favorable electrical and mechanical properties, making it suitable for use in FED vacuum spacers.

1. Introduction

Because field emission displays (FED) require a high-vacuum operation condition to optimize the life-time of electron field-emitters,[1,2] vacuum spacers,[3] which keep the phosphor anode and the emitter cathode separated at a fixed distance, are used to withstand the atmospheric pressure. The vacuum spacers should be able to sustain high voltage between the two electrodes without electrical breakdown.[4,5] Therefore, vacuum spacers must be composed of electrically insulating materials exhibiting a strong mechanical strength. For satisfactory image brightness, the two electrodes are biased at a high voltage so that the field-emitted electrons of high energy can effectively excite the phosphor anode plate.[6,7] However, when field-emitted electrons bombard the phosphor plate, the resulting backscattered electrons may strike the spacers, resulting in secondary electron (SE) emission from the spacers. Because most dielectric materials have an SE emission coefficient larger than one, the spacers gradually become positively charged during FED operation. Charged spacers can significantly alter the local electric field near the spacer, thus changing electron trajectories from the cathode to the anode plates,[8–10] resulting in image distortion for those pixels near the FED spacers.[11] Hence, SE emission from the spacer must be minimized for favorable FED performance. One approach to suppressing the SE emission is to prepare a surface that can effectively trap escaping secondary electrons. For example, a rough surface or a porous structure can substantially reduce secondary electron emission.[12–15] In this study, we fabricated porous anodic aluminum oxide (AAO) overlayers on glass spacers to suppress SE emission.[16,17] Because carbon has a low SE yield,[18] we deposited a carbon thin film on the AAO overlayer to reduce the SE emission further. The SE emission efficiency of the porous overlayers was evaluated by using an Auger electron microscope.

2. Experiment

Figure 1 schematically illustrates the setup of the Al anodization. Two electrochemical setups were used to prepare the AAO overlayer. For the study on secondary electron emission from the AAO overlayer, the anodization area of the Al thin film was limited to a circular area that was 1.5 cm in diameter, which was determined according to the open circular window of an acrylic container filled with an aqueous H_3PO_4 solution. The open window allowed a large portion of the Al thin film to be immersed in the electrolyte. A Pt disk (1 cm in diameter) was used as the counter electrode. The other setup was designed to fabricate AAO overlayers simultaneously on both sides of a glass plate with an area of $2 \times 10\,cm^2$, as well as to determine the feasibility of the AAO spacer fabrication method for practical FED applications. Two rectangular Pt wire loops were firmly pressed to the periphery of both sides of the Al-coated sample by using two Teflon masks to ensure a uniform potential distribution on the sample. The Teflon masks have a large rectangular open area of $\sim 1.8 \times 9.5\,cm^2$ for Al anodization in the H_3PO_4 solution. Two graphite plates with dimensions similar to that of the sample were used as the

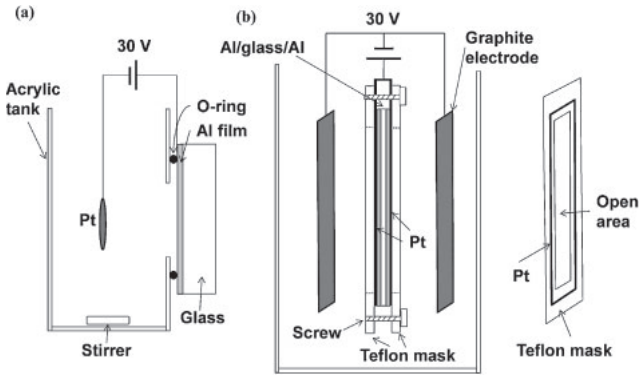

Fig. 1. The setups of Al anodization for fabrication of (a) circular AAO overlayers with a diameter of 1 cm, and (b) rectangular AAO overlayers with a size of $2 \times 10\,cm^2$. The large sample setup are for Al anodization on both sides of the glass substrate; two graphite counter electrodes were used for two-side anodization. The drawing on the right is the tilting view of the Teflon mask.

counter electrode. To fabricate the AAO-coated glass plate, we first deposited a 1-μm-thick aluminum thin film on both sides of the glass plate by performing electron beam evaporation (e-beam), followed by thermal annealing at 400 °C in a vacuum. Anodic oxidation of the Al film was conducted in a 10% v/v aqueous solution of phosphoric acid (H_3PO_4) at 10 °C and at a constant polarization voltage of 30 V. The end point of the anodization process was determined according to the drastic drop of the anodic current, which was monitored by using a Keithley 2400 measurement system. The electrolyte was gently stirred using a small magnet bar during the Al anodization. To minimize secondary emission from the AAO, we deposited an ultra-thin carbon film on the AAO overlayer. The carbon film was deposited by using a carbon evaporator (JOEL JEC-560), which had a base pressure of 2×10^{-2} Torr. Under the evaporation condition with the heating voltage set at 4.5 V, the carbon deposition rate was 1.4 Å/s.

The crystallinity of the Al and AAO thin films was studied by performing X-ray diffractometry (XRD; Bruker AXS Advance D8) and using Cu Kα radiation as the excitation source. The surface morphology of the samples was examined by scanning electron microscopy (SEM; JEOL JSM-6700F). The adhesion strength of the AAO overlayers with the glass substrate was determined by a pull-off adhesion tester (Romulus III). The electrical resistance of the spacer samples was measured by a source-measure unit (Keithley 237). The relative SE efficiency of the porous samples was measured in an Auger electron spectrometer (Thermo VG 350); the incident electron beam energy was 10 keV and the beam current was 5 nA. Electrons emitted from the samples were collected by a stainless steel grid, which was welded on the periphery of the sample holder, which was biased at 0–20 V. The SE current measurement is described in greater detail in the discussion section.

3. Results and Discussion

Figures 2(a)–2(f) show SEM images of the AAO samples prepared in this study. The SEM images shown in Figs. 2(a) and 2(b) are for the as-prepared AAO overlayer, which was produced at 10 °C and at 30 V, using the electrochemical setup for small circular samples (1.5 cm in diameter). The AAO overlayer exhibits a random pore arrangement on the surface as shown in the plane-view SEM image. The development of the irregular arrangement is because the AAO overlayer was produced by performing one-step anodization, which produced random pits on the Al film surface at the beginning of the polarization process. As shown in Fig. 2(b), the cross-sectional SEM image shows that the random pits gradually develop into a pore channel array, which extends downward to the interface between the Al thin film and the glass substrate. The pore channels have a diameter of ~80 nm. The pore density is $\sim 1.7 \times 10^{10}$ pores/cm^2, which corresponds to a porosity of ~85% in the AAO overlayer (assuming a through pore structure). When a large (2×10 cm^2), rectangular Al thin film is anodized under the same anodization condition as that of the small circular thin film, a pore channel array structure can also be produced, as shown in Figs. 2(c) and 2(d). The surface of the large sample is more porous than that of the small sample. However, the cross-sectional image in

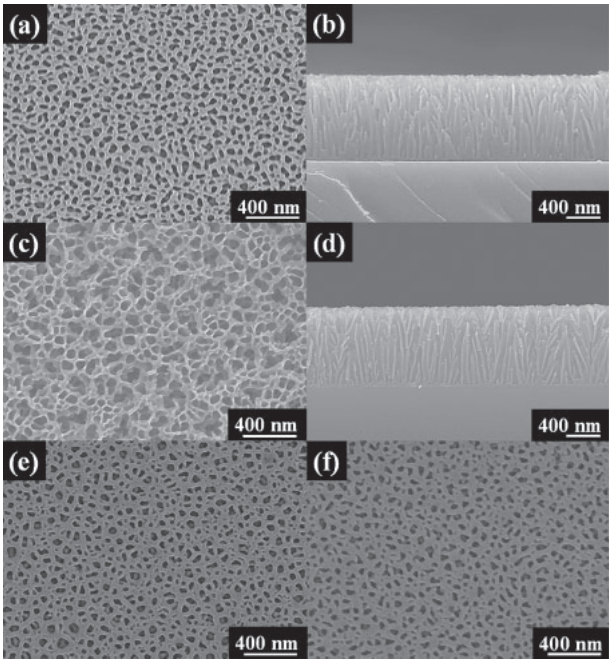

Fig. 2. Plane-view (a) and cross-sectional (b) SEM images of the circular AAO overlayer; plane-view (c) and cross-sectional (d) SEM images of the rectangular AAO overlayer; plane view SEM images of (e) the AAO-25C sample and (f) the AAO-50C sample.

Fig. 2(d) shows that the large sample has a similar uniform distribution of AAO pore channels to that of the small sample. By examining various areas on the large AAO-coated sample, we found that the thickness of the AAO overlayer was uniform over the glass plate. Because one-step anodization was used to prepare the AAO overlayers and the Al thin films received no surface pretreatment before anodization, the pore channels in the AAO overlayers were not well aligned. However, for the purpose of the vacuum spacer application, a well-aligned pore-channel structure was unnecessary. The success of the fabrication of the uniform AAO overlayer on a large substrate suggested that the Al anodization process can be used for commercial vacuum spacers, which may be as large as $\sim 130 \times 2$ mm^2 in size. A strong adhesion between the AAO overlayer and the glass substrate is essential to the practical application of the overlayer for FED technology, because the presence of debris caused by the cracking or peeling of an overlayer may catastrophically damage the FED. In this study, we used a pull-off adhesion tester to measure the adhesion strength of the AAO overlayer with the glass substrate; the measured adhesion of the AAO overlayer was ~20 kg/cm^2, which should be durable for use of FED spacers. Although the adhesion strength of the overlayer is critical, it is the bulk mechanical strength of the spacer that plays the decisive role in supporting the screen against atmospheric pressure. Because we successfully fabricated AAO on various oxide substrates, such as SiO_2 and Al_2O_3, depositing the AAO overlayer on commercial FED spacers, which are generally made of alumina or glass plates, should be of little difficulty. Therefore, an AAO-coated FED spacer must have a mechanical strength similar to a bare spacer.

Because an FED spacer must have an extremely high electrical resistivity to prevent the electrical breakdown

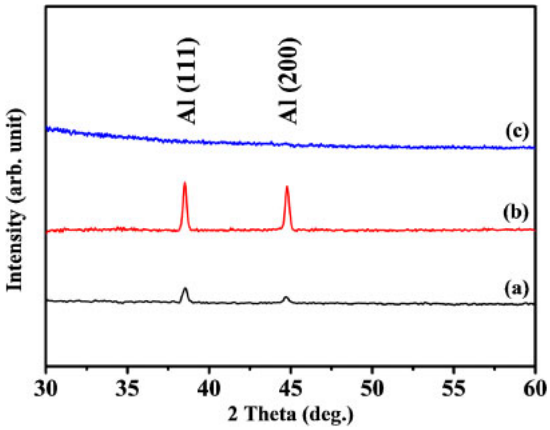

Fig. 3. (Color online) XRD spectra of (a) the as-deposited Al thin film, (b) the 400 °C-annealed Al thin film, and (c) the as-prepared AAO overlayer.

between the anode and the cathode, which are biased at an extremely high voltage (~10 kV), the porous AAO overlayer on the glass substrate must be free from continuous metallic residues. Therefore, the Al thin film must be consumed as completely as possible at the end of the AAO overlayer fabrication. If any metallic residues remain in the overlayer after the anodization process, it must be isolated from the peripheral region of the spacer, where the spacer is electrically contacted with the anode and the cathode. To determine if any metallic residue remained in the as-prepared spacer, we used grazing angle XRD to analyze chemical phases present in the spacers. Figure 3 shows XRD spectra of the Al and porous AAO films. For the as-prepared Al thin film (Curve a), the two diffraction peaks situated at 38.6 and 44.6° are due to the cubic Al(111) and (200) lattice planes, respectively. After the vacuum annealing of the Al film at 400 °C for 1 h (Curve b), the (111) and (200) peaks became much higher and sharper, indicating that the thermal annealing improved the crystallinity of the Al thin film. The XRD spectrum was featureless after Al anodization, indicating that the Al thin film was converted into an amorphous AAO overlayer. However, because of the shallow probe depth and poor detection limit, the results of grazing angle XRD analysis cannot negate the possible presence of trace metallic Al residues at the interface between the AAO overlayer and the glass substrate. Isolated metallic Al residues is usually present at the interface between the substrate and the alumina barrier layer, which is formed during Al anodization.[19] The variation in the pore-channel depth in a large AAO sample can leave a significant amount of aluminum residues at the interface between the AAO overlayer and the glass substrate.[20] Thermal annealing of the AAO spacer in air at high temperatures can be used to oxidize interfacial metallic residues, if any, on the periphery of the spacer. To measure the resistance of the spacers, we attached two pieces of Cu tape (as the contact electrodes) to the rims of the small circular sample, and both contacts were 5 mm apart. After thermal oxidation, the electrical resistance of the as-prepared AAO spacer was in the order of 10^{10} Ω, indicating that the AAO overlayer was likely free from continuous electrical conducting residue that can lead to electrical breakdown. The large rectangular spacer must have a larger resistance as well because it is ten times longer than the smaller circular sample.

Alumina has a large secondary electron yield;[21] therefore, secondary electron emission from the AAO overlayer resulting from electron bombardment induces positive charges on the surface. To minimize the positive charge effect, we evaporation-deposited a carbon thin film on the AAO overlayer because carbon has a low SE yield.[18] Figure 2(e) shows the plane-view SEM image of the AAO overlayer capped with a carbon thin film, which was deposited for 25 s. We refer to the carbon-coated AAO sample as "AAO-25C" hereafter. Under the carbon coating condition, the carbon deposition rate on a thermal SiO_2 substrate was 1.4 Å/s, according to SEM analysis; the average thickness of the carbon layer on the AAO-25C samples was thus estimated at ~3.5 nm. The AAO pore size decreased after the carbon deposition, suggesting that the carbon deposit spread into the AAO pore channels, thereby reducing the open area of the pores. When the carbon deposition time was increased to 50 s, the pore size of the AAO overlayer (denoted by AAO-50C) was further decreased, as shown in Fig. 2(f). The change in pore size has a significant influence on the secondary electron emission efficiency, as discussed below. Ensuring that the carbon-coated AAO spacers have a resistance sufficiently high for meeting the electrical requirement for FED spacers in crucial. Carbon films generally have an electrical resistivity varying over a wide range of values, from 10^2 to 10^{16} Ω cm, depending on the preparation condition.[22] We deposited continuous carbon thin films on a thermal SiO_2 substrate and measured the electrical resistance of the carbon films; the resistance was in the order of 10^{10} Ω/cm, indicating that the carbon films prepared under the present deposition condition are highly electrically resistive. The measured resistance of the AAO-25C and AAO-50C samples were 2.23×10^{10} and 1.39×10^{10} Ω, respectively. The high electrical resistance of both the carbon coated AAO samples is desirable for the use of FED spacers. However, the measured high electrical resistance of the carbon-coated samples does not ensure their reliability during FED operations because isolated conductive clusters, which might have escaped from detection in this study, can result in catastrophic electrical breakdown under the high-voltage operation condition.[23] Further high-voltage breakdown tests under a high-vacuum condition are required.

The SE efficiency of the AAO overlayer was evaluated by using a scanning Auger electron microscope (SAM). Because the SAM system allows only a sample size smaller than 1 cm in diameter, the smaller AAO samples were used for the SE efficiency evaluation. As depicted in Fig. 4, the AAO samples were placed on a Teflon disk, which was attached to a circular stainless steel sample holder. The holder has stainless steel grids on the periphery and was positively biased at 0–20 V. The electron beam of 10 keV was incident normally on the AAO sample, and secondary electrons were collected by the grids. Because secondary electrons have a maximal energy distribution below 10 eV, most of the secondary electrons emitted from the AAO surface will be collected by the grids that are biased at a potential larger than 10 V. Backscattered electrons may also be emitted from the sample surface during electron

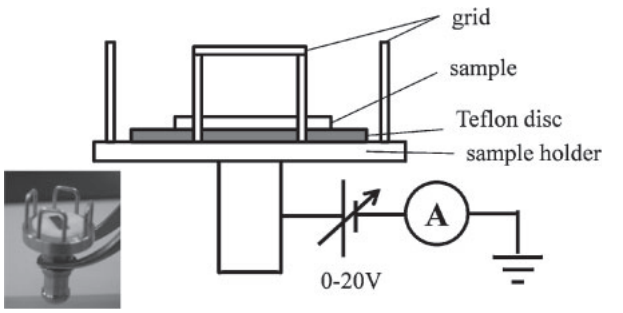

Fig. 4. The measurement setup for secondary electrons emitted from the AAO sample.

bombardment. However, the majority of backscattered electrons can escape from the positive potential trap confined by the grids because they generally have a kinetic energy much larger than 20 eV. Although the measurement setup is incapable of measuring the absolute SE yield, it is reasonably suitable for the comparison between the samples in the relative secondary electron yield. Figure 5 shows the measured current of electrons emitted from the as-prepared AAO, AAO-25C, and AAO-50C samples at various bias potentials as a function of the measurement time. The AAO-25C sample exhibits the lowest SE efficiency among the three tested samples. The measured currents at 0 and 5 V are nearly the same for all three samples, suggesting that the grid cannot effectively collect the emitted electrons under the low bias condition. When the bias potential is increased to 10 V, both the AAO and AAO-50C samples have a measured current of ~0.6 nA, whereas the AAO-25C has a stable current of ~0.3 nA. When the sample holder is biased at a potential larger than 15 V, the measured current for the AAO and AAO-50C samples is increased dramatically (~2 nA at 15 V and >4.5 nA at 20 V). By contrast, the AAO-25C has a stable low current of 0.5 nA at 15 V and of 0.8 nA at 20 V. For comparison, we have also performed the SE emission measurement for a commercial FED spacer that is made of alumina. At a grid bias larger than 15 V, the SE emission current of the spacer is about 1.75 times that of the carbon coated AAO sample.

The smaller secondary electron emission for the AAO-25C sample may be ascribed to a thicker pore wall than that of the as-prepared AAO sample and the small SE yield of carbon. The carbon deposit on the AAO-25C sample increases the wall thickness of the pore channels in the surface region, as demonstrated by the smaller pore size shown in Fig. 2(e); thus, the carbon deposit can effectively retard the escape of secondary electrons produced in AAO pore walls. Figure 6 schematically illustrates possible trajectories of secondary electrons emitted from the surface and pore walls of the AAO overlayer. Secondary electrons (or backscattered electrons of low energy) produced in AAO pore walls must travel a longer distance (as a result of the carbon coating) to escape from the AAO-25C sample than those from the as-prepared AAO sample; therefore, fewer electrons were measured for the AAO-25C sample. Most escaping secondary electrons are likely from the carbon capping layer, which has a lower SE yield than alumina does. Moreover, as illustrated in Fig. 6, it is more efficient for a thicker pore wall than for a thinner pore wall to trap

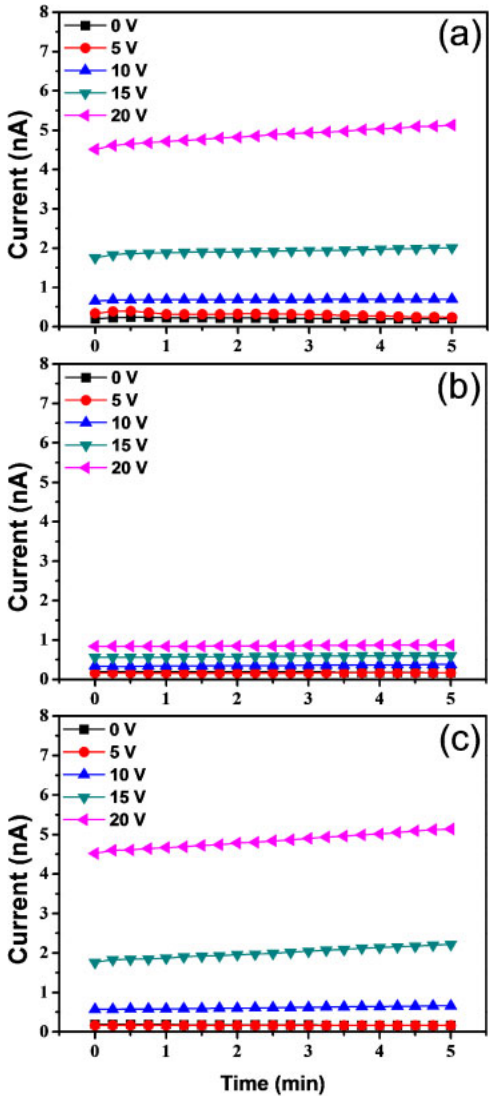

Fig. 5. (Color online) Secondary electron currents collected by the grids on the sample holder at different biased potentials as a function of the measurement time: (a) the as-prepared AAO overlayer, (b) the AAO-25C sample, and (c) the AAO-50C sample.

secondary electrons emitted from a neighboring pore wall at in an inclined angle (indicated by the dashed line). As a result, the AAO-25C sample had a smaller measured emission current. However, the heavy carbon deposition for the AAO-50C sample appears to be of little benefit in reducing the SE yield; this is likely because the heavy carbon deposition on the AAO surface modifies the surface morphology of the sample. The SEM image in Fig. 2(f) indicates the significant decrease in the pore size of the AAO overlayer after the carbon deposition of 50 s. The decrease in the AAO pore size increases the surface area that is subject to direct electron bombardment; thus AAO sample may have a poor suppression of secondary electron emission because the majority of secondary electrons produced in the surface region can easily escape from the AAO-50C sample. The reduction in the SE trapping efficiency caused by the smaller pore size may offset the benefit of the low SE yield of the carbon deposit. Based on the SE measurement results, effectively suppressing the secondary emission from a porous AAO spacer requires optimizing the amount of carbon deposited on the spacer.

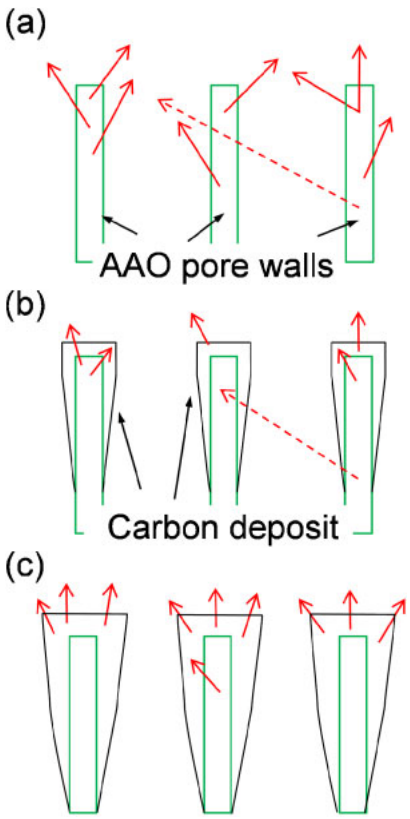

Fig. 6. (Color online) Schematic illustration for the trajectory of secondary electrons emitted from the AAO overlayer: (a) the as-prepared AAO overlayer, (b) the AAO-25C sample, and (c) the AAO-50C sample. The arrows depict trajectories of secondary electrons emitted from the surface and pore walls of the AAO overlayer; the dashed arrows represent secondary electrons emitted in an inclined angle that causes the electrons to strike neighboring pore walls.

4. Conclusions

We fabricated porous AAO overlayers on glass substrates to examine the effect of carbon deposition on the reduction of SE emission from the AAO overlayers. AAO overlayers with a uniform pore-channel distribution can be simultaneously prepared on both sides of a glass plate $2 \times 10\,\mathrm{cm}^2$ in size, suggesting that the Al anodization approach is applicable to the surface modification of FE-FPD vacuum spacers. The relative SE emission efficiency of the AAO overlayer was evaluated by extracting emitted electrons of low energy with the grid biased at 0–20 V. For the three samples prepared in this study, that with a carbon deposition of 25 s exhibits the lowest SE emission. We ascribe the low SE emission of the AAO-25C sample to the low SE yield of the carbon deposit and a thicker AAO pore wall, which suppresses the SE escaping from the pore channels. The AAO-50C sample has a smaller pore size and, thus, has a larger wall thickness in the surface region than the other two samples as a result of the heavy carbon deposition. The increase in the pore wall thickness in the surface region of the AAO-50C sample increases the electron bombardment area, thereby enhancing secondary electron emission. The adhesion strength and electrical resistance measurements indicates that the carbon coated AAO is suitable for use as a spacer overlayer for FED applications.

Acknowledgments

We thank the AU Optronics Corporation for the financial support. The technical support of the National Nano Device Laboratories is also gratefully acknowledged.

1) S.-H. Yang, J.-H. Syu, Y.-M. Hsu, and W.-M. Chuang: Jpn. J. Appl. Phys. **51** (2012) 115001.
2) W.-C. Shih, J.-M. Jeng, C.-W. Tsou, J.-T. Lo, H.-C. Chen, and I.-N. Lin: Jpn. J. Appl. Phys. **49** (2010) 08JF11.
3) Y.-R. Cho, H.-S. Kim, J.-Y. Oh, J.-D. Mun, J.-O. Choi, J. H. Lee, K.-I. Cho, and S. Ahn: Mater. Sci. Eng. B **77** (2000) 6.
4) X. Ma and T. S. Sudarshan: IEEE Trans. Dielectr. Electr. Insul. **7** (2000) 277.
5) X. Ma and T. S. Sudarshan: J. Vac. Sci. Technol. B **19** (2001) 683.
6) C.-C. Kao and Y.-C. Liu: Mater. Chem. Phys. **115** (2009) 463.
7) C. C. Kang and R. S. Liu: J. Lumin. **122–123** (2007) 574.
8) Y. S. Choi, S. N. Cha, S. Y. Jung, J. W. Kim, J. E. Jung, and J. M. Kim: IEEE Trans. Electron Devices **47** (2000) 1673.
9) L. Wei, X. Zhang, C. Lou, and Z. Zhu: Appl. Surf. Sci. **254** (2008) 2096.
10) P. Lunliang, L. Jie, and C. Jun: presented at 22nd Int. Vacuum Nanoelectronics Conf., 2009.
11) H. Hao, P. Liu, J. Tang, Q. Cai, and S. Fan: Carbon **50** (2012) 4203.
12) M. Pivi, F. K. King, R. E. Kirby, T. O. Raubenheimer, G. Stupakov, and F. Le Pimpec: J. Appl. Phys. **104** (2008) 104904.
13) H. Bruining: *Physics and Applications of Secondary Electron Emission* (Pergamon, London, 1954).
14) O. Yamamoto, T. Takuma, M. Fukuda, S. Nagata, and T. Sonoda: IEEE Trans. Dielectr. Electr. Insul. **10** (2003) 550.
15) S. W. Lee, Y. J. Baik, C. J. Kang, and D. Jeon: Appl. Surf. Sci. **215** (2003) 265.
16) B. Wang, G. Xu, and P. Cui: Mater. Lett. **93** (2013) 36.
17) C. K. Y. Ng and A. H. W. Ngan: Chem. Mater. **23** (2011) 5264.
18) C. Y. Vallgren, G. Arduini, J. Bauche, S. Calatroni, P. Chiggiato, K. Cornelis, P. C. Pinto, B. Henrist, E. Métral, H. Neupert, G. Rumolo, E. Shaposhnikova, and M. Taborelli: Phys. Rev. ST Accel. Beams **14** (2011) 071001.
19) P.-L. Chen, C.-T. Kuo, F.-M. Pan, and T.-G. Tsai: Appl. Phys. Lett. **84** (2004) 3888.
20) P. G. Miney, P. E. Colavita, M. V. Schiza, R. J. Priore, F. G. Haibach, and M. L. Myrick: Electrochem. Solid-State Lett. **6** (2003) B42.
21) H. Seiler: J. Appl. Phys. **54** (1983) R1.
22) A. Grill: Thin Solid Films **355–356** (1999) 189.
23) R. V. Latham: *High Voltage Vacuum Insulation: Basic Concepts and Technological Practice* (Academic Press, New York, 1995) p. 229.